Journal of Non-Crystalline Solids 609 (2023) 122267

Contents lists available at ScienceDirect

Journal of Non-Crystalline Solids

journal homepage: www.elsevier.com/locate/jnoncrysol

Effect of thermal treatments below devitrification temperature on the magnetic and magnetocaloric properties in mechanically alloyed $Fe_{70}Zr_{30}$ powders

A.F. Manchón-Gordón [a,*], J.S. Blázquez [b], M. Kowalczyk [c], J.J. Ipus [b], T. Kulik [c], C.F. Conde [b]

[a] Instituto de Ciencia de Materiales de Sevilla, ICMSE CSIC-Universidad de Sevilla, C. Américo Vespucio 49, Sevilla 41092, Spain
[b] Dpto. Física de la Materia Condensada, ICMSE-CSIC, Universidad de Sevilla, P.O. Box 1065, 41080 Sevilla, Spain
[c] Faculty of Materials Science and Engineering, Warsaw University of Technology, 141 Wołoska st., 02-507 Warsaw, Poland

ARTICLE INFO

Keywords:
Amorphous structure
Relaxation phenomena
Mössbauer spectroscopy
Magnetic inhomogeneity
Magnetocaloric properties

ABSTRACT

In this work, the relaxation of the amorphous structure of mechanically alloyed $Fe_{70}Zr_{30}$ powders has been analyzed through interrupted heating ramps below the devitrification temperature. As a result of such thermal treatment, Curie temperature and temperature at maximum magnetic entropy change curves shift to higher temperatures as the temperature of heating treatment increases. This effect can be attributed to both the release of the stress accumulated in the amorphous powder during the milling process and to the initiation of nucleation of α-Fe crystallites, as it has been shown by Mössbauer spectroscopy.

1. Introduction

Magnetic properties of Fe-rich amorphous alloys have received significant attention in the research community from both fundamental and technological perspectives [1,2]. These materials present atypical magnetic phenomena, such as magnetoelastic behavior [3] or double transition behavior [4], depending on Fe content [5] and the local atomic order [6]. Moreover, these systems can be also considered as a precursor for the development of different intermetallics [7]. Furthermore, these amorphous soft ferromagnetic alloys have received considerable attention in the research community focused on magnetocaloric effect, MCE, and magnetic refrigeration at temperatures close to room temperature [8]. Soft magnetic amorphous alloys can be classified as magnetocaloric materials with a second order magnetic transition (SOPT). Although the MCE exhibited by these systems is not really in competition with Gd (paradigmatic material for magnetic refrigeration at room temperature [9]) or systems with a first order magnetic transition, such as Ni-based Heusler alloys [10], they exhibit a really reduced magnetic hysteresis and an easily tunable Curie temperature with small compositional changes [11,12]. Furthermore, the field dependence of MCE for these systems is well established [13].

Although amorphous alloys are typically produced by rapid quenching techniques, the existence of two eutectic points in the Fe-Zr phase diagram [14,15] restricts the capability of this technique to produce amorphous alloys to specific compositions, close to $Fe_{25}Zr_{75}$ and $Fe_{90}Zr_{10}$. Thus, other techniques have been proposed to prepare amorphous Fe-Zr compounds in a broader range of compositions, such as mechanical alloying or sputtering techniques, which expand the production of amorphous samples for a Fe content of 30–80 at.% [16] and 20–90 at.% [17], respectively.

The mechanical alloying technique has been employed to produce many amorphous alloys [18] and, generally, leads to strongly disordered systems. Consequently, the milled amorphous samples are in a metastable state, which can induce different transformations during thermal treatments, even at temperatures lower than those corresponding to the devitrification process. Although some works pay attention to the $Fe_{70}Zr_{30}$ at.% amorphous alloy [5,19-21] and its devitrification process [7], including some previous works of the authors [22–24], the study of the effect of the relaxation phenomena on the magnetic behavior of this alloy has not yet been performed.

The purpose of this study is to analyze the effect of the relaxation phenomena of amorphous $Fe_{70}Zr_{30}$ powders prepared by mechanical alloying on their magnetic behavior. Therefore, to shed some light on the metastable character of these samples, the present work is devoted to analyze the thermal dependence of the magnetic properties of the alloy submitted to different thermal treatments at temperatures below the devitrification temperature.

The results obtained in this study are complementary to earlier works

* The corresponding author.
E-mail address: afmanchon@us.es (A.F. Manchón-Gordón).

https://doi.org/10.1016/j.jnoncrysol.2023.122267
Received 23 January 2023; Received in revised form 2 March 2023; Accepted 6 March 2023
Available online 14 March 2023

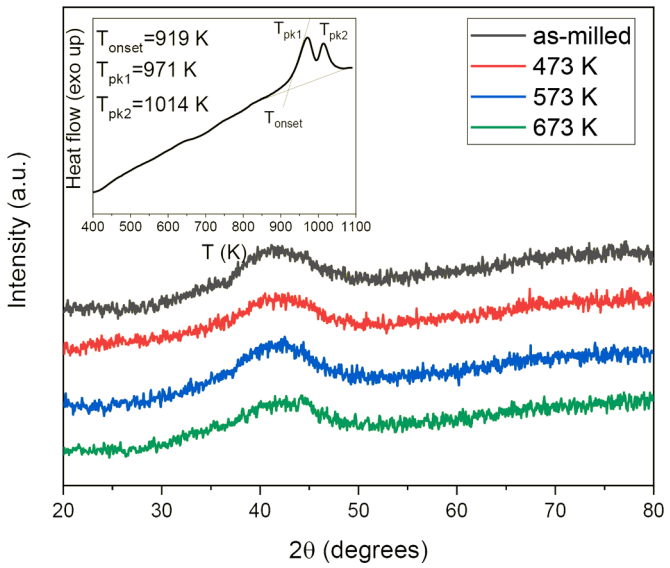

Fig. 1. XRD patterns at room temperature of $Fe_{70}Zr_{30}$ as-milled amorphous alloy and after heating up to the marked temperatures. Inset shows DTA curves of the devitrification of the as-milled amorphous alloy under a constant heating rate of 10 K/min. Characteristic temperatures, onset, T_{onset}, and peak temperatures, T_{pk}, have been indicated.

of the authors on the Fe-Zr amorphous alloys prepared by mechanical alloying in which several aspects have been investigated: i) the evolution of Fe environments and the phase composition during mechanical amorphization process [25]; ii) the kinetics of the mechanical amorphization [26]; iii) the influence of milling time on the magnetic properties [27]; and iv) the thermal stability and the kinetics of crystallization [7].

2. Experimental

Amorphous alloy with $Fe_{70}Zr_{30}$ at.% composition was synthesized by mechanical alloying. Details on preparation and a detailed analysis of the microstructure of the synthesized powders can be found in ref. [25]. After 50 h of milling, mechanical alloying results in the alloy with amorphous structure. To explore the effect of heating on the amorphous structure, powder samples were heated, at 10 K/min up to different maximum temperatures in a differential thermal analysis (DTA) Perkin-Elmer DTA7 unit under Ar flow. Three different maximum temperatures were reached in the experiments performed: 473, 573 and 673 K. Subsequently, the samples were cooled down to room temperature inside the oven.

Two techniques confirmed the amorphous character of the powder: X-ray diffraction using Cu-Kα radiation in a Rigaku MiniFlex diffractometer and DTA. Transmission Mössbauer spectra were measured using a ^{57}Co(Rh) source at room temperature and fitted with NORMOS program [28]. Isomer shift has been given relative to an α-Fe foil at room temperature. Samples for Mössbauer spectroscopy were prepared by spreading powder on a Fe-free adhesive tape in such a way that the thickness of the sample is of the order of that of the Fe thin foil standard used for calibration. Therefore, thin absorber approximation was used for the fitting of the spectra.

Temperature and magnetic field dependent magnetization were obtained using the vibrating sample magnetometer standard option of a Physical Properties Measurements System (PPMS, Quantum Design) between 100 and 400 K in the applied field range of ±1.5 T. Loose powder was packed in the VSM powder Sample Holders. Effect of demagnetizing factor has not been considered in this study.

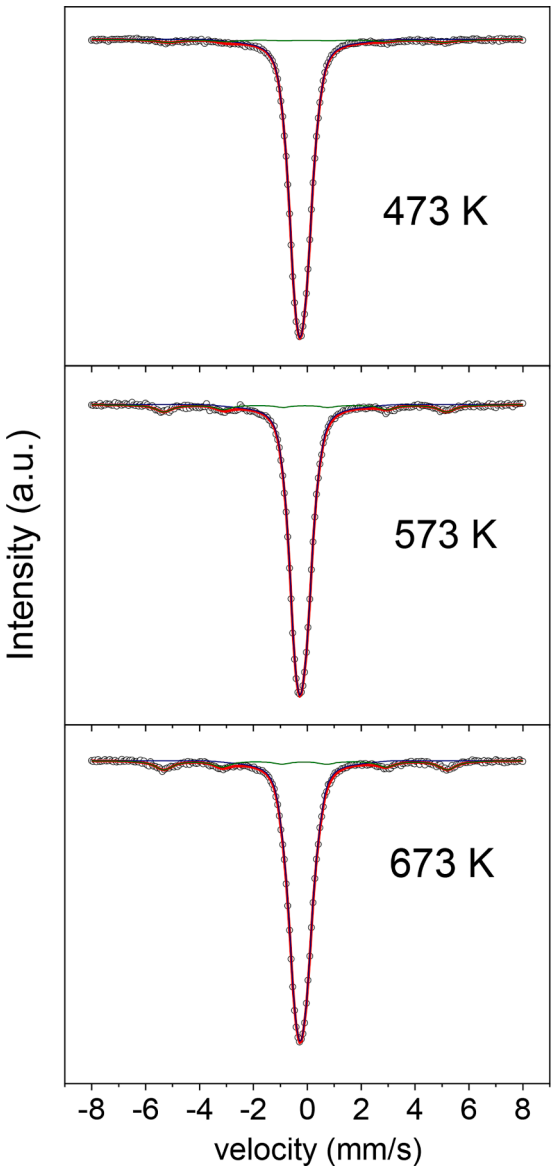

Fig. 2. Mössbauer spectra at room temperature for amorphous samples after heated up to the marked temperatures.

3. Results and discussion

Fig. 1 depicts the XRD patterns taken at room temperature from powders heating up to the indicated temperatures below the devitrification temperature, as observed in the inset. This inset shows the DTA scans of the as-milled powder at 10 K/min, where an onset temperature ~920 K can be observed. The two peaks detected correspond to the formation of the Fe_2Zr and $Fe_{23}Zr_6$ intermetallics [7]. Despite of the heating treatment, the amorphous structure is retained, as can be inferred by the existence of a broad halo at $2\theta \sim 43^\circ$ in all the studied conditions. In the case of 573 and 673 K annealing temperatures, a small diffraction peak begins to develop located at around $2\theta \sim 45^\circ$, associated with the (110) maximum diffraction peak of the α-Fe phase. Although the XRD pattern of the as-milled and 473 K annealing temperature do not exhibit the presence of α-Fe crystallites in the sample, it has been shown the existence of residual α-Fe nanocrystals by Mössbauer spectroscopy at low temperatures in the as-milled powders (~3% phase contribution) [27]. The ferromagnetic character of the amorphous matrix at temperatures below room temperature allows for a ferromagnetic coupling between the residual α-Fe crystallites and the visible

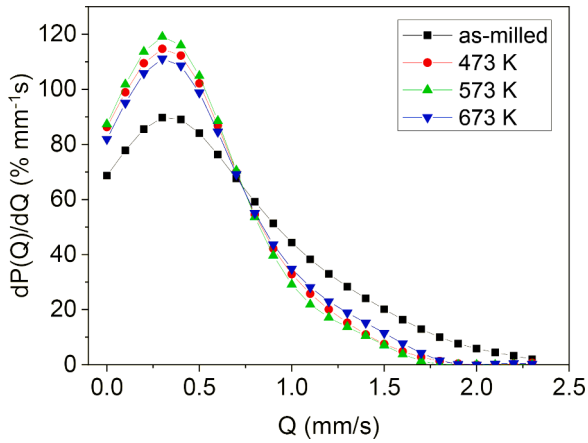

Fig. 3. Probability distribution of quadrupole splitting for the studied powders.

Table 1
Hyperfine parameters of the studied thermally treated amorphous samples. Area (%) is the relative contribution of the component, and B_{hf} and δ are the values of the hyperfine magnetic field and the isomer shift of the ferromagnetic site, respectively. $<Q_s>$ is the mean value of the quadrupolar shift.

Annealing temperature (K)	Component	Area (%)	B_{hf} ±0.1 (T)	δ±0.02 (mm/s)	$<Q_s>$±0.05 (mm/s)
473	Quadrupolar distribution	94	–	−0.15	0.49
	α-Fe site	6	31.6	0.06	–
573	Quadrupolar distribution	90	–	−0.14	0.47
	α-Fe site	10	32.5	0.04	–
673	Quadrupolar distribution	88	–	−0.14	0.52
	α-Fe site	12	32.6	0.02	–

contribution by Mössbauer spectroscopy. Therefore, the appearance of the (110) maximum diffraction peak in the case of 573 and 673 K annealing temperature correspond to an increase of the crystal size of those remaining crystallites in the amorphous matrix.

Fig. 2 presents Mössbauer spectra taken at room temperature of the alloy powders heated up to the marked temperatures. As the annealing temperature increased, an increase of the peaks around ±4 and ±6 mm/s can be observed, indicating the development of a magnetically-ordered phase at room temperature. Consequently, two components have been employed to fit the spectra, a quadrupolar distribution and a ferromagnetic sextet. While the first paramagnetic contribution can be ascribed to the amorphous phase, the ferromagnetic site can be associated with the formation of the α-Fe phase, characterized by a hyperfine field of about 33 T. The quadrupole splitting distributions, $P(QS)$, are displayed in Fig. 3, which exhibit the same behavior for all the samples, with a non-zero probability for QS=0 mm/s. The obtained hyperfine parameters from the spectra fitting have been collected in Table 1. The mean value of quadrupole splitting, $\langle QS \rangle$, is close to the values previously reported for as-milled $Fe_{70}Zr_{30}$ alloy $\langle QS \rangle$=0.53±0.07 mm/s [25]. Despite the development of the α-Fe phase and the corresponding Fe impoverishment of the amorphous alloy, no significant effects on the quadrupolar distribution have been detected.

From these fits, an evident increase of the ferromagnetic contribution with the increase of the temperature of treatment can be observed, reaching a value of 12% of the total Fe atoms in α-Fe sites for the case of the annealed powder at 673 K (assuming pure α-Fe, this yields 8.5 atomic fractions for the crystalline phase). Even though the α-Fe phase was not detected by XRD, the existence of this phase is evident by the Mössbauer spectra of the analyzed powders. The formation of the α-Fe

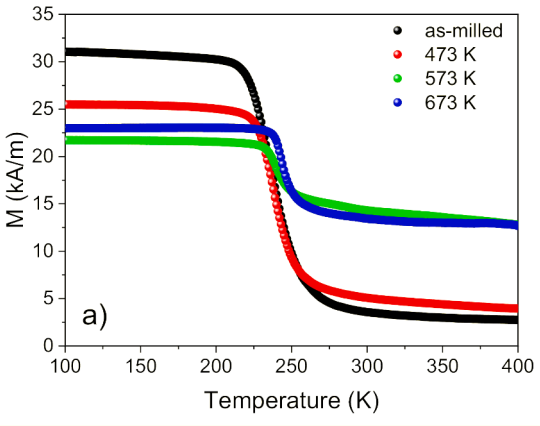

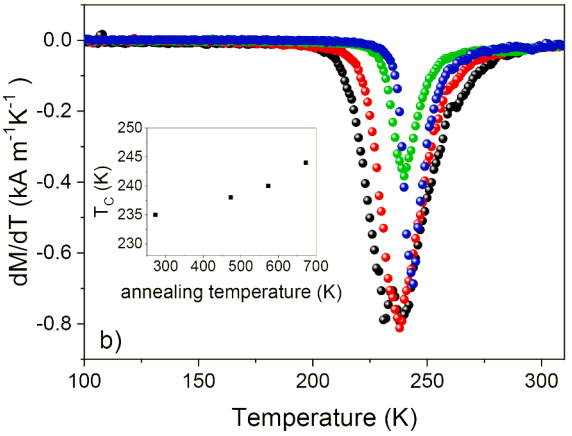

Fig. 4. a) Temperature dependence of the specific magnetization of $Fe_{70}Zr_{30}$ as-milled amorphous alloys and after heating up to the marked temperatures under an applied magnetic field of 100 Oe. b) Corresponding dM/dT curves. Inset shows the evolution of the Curie temperature obtained as the minima of dM/dT curves. The corresponding data for the as-milled sample has been included for comparison.

phase at temperatures lower to the crystallization temperature of the amorphous alloy is due to the existence of residual α-Fe crystals after the amorphization process. Although these nanocrystals can not be detected by XRD technique at room temperature, their existence is clearly confirmed when the samples are analyzed by Mössbauer spectroscopy at temperatures below room temperature. In fact, at room temperature, the paramagnetic character of the amorphous matrix prevents the coupling of the disseminated α-Fe nanocrystals. Moreover, it is well known that Mössbauer spectroscopy is a more precise technique than XRD to identify Fe-rich phases [25], particularly in such cases as the one analyzed here, where the amorphous halo can jeopardize the presence of tiny but broad crystalline maximum. On the other hand, an increase of the hyperfine field of the sextet assigned to the α-Fe phase have been also determined. This evolution can be associated with the decrease of Zr atoms in the neighborhood of the α-Fe phase. It has been shown that the hyperfine field of Fe is strongly affected by the presence of other atoms as a near neighbors (e.g. $\Delta B_{hf} \sim -3$ T for a non-magnetic atom in the two first shells [29]).

Fig. 4a illustrates the magnetization dependence on the temperature of the studied powders when an external magnetic field of 100 Oe is applied. On cooling, the thermomagnetic curves are characterized by a sudden increase of the magnetization around 240 K, corresponding to the paramagnetic to ferromagnetic phase transition of the amorphous phase. It indicates the paramagnetic behavior of the amorphous powder at room temperature, in agreement with the Mössbauer spectroscopy

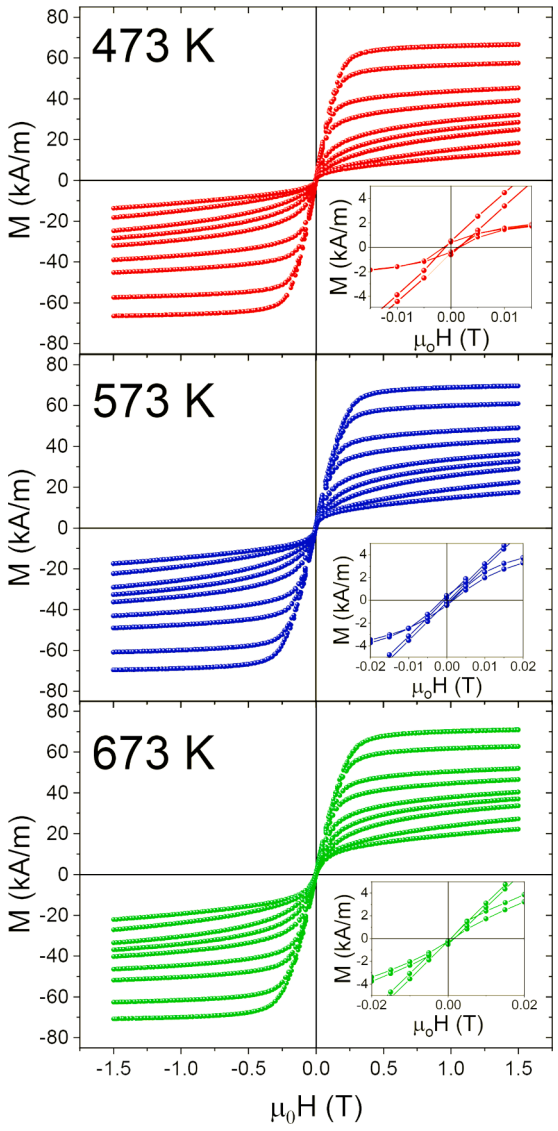

Fig. 5. Magnetic hysteresis loops, taken at different temperatures from 100 K to 300 (100, 150, 200, 220, 240, 250, 260, 280 and 300 K) of the mechanically alloyed powders after heating up to the indicated temperatures. Insets show the low field region of the hysteresis loops at 100 and 300 K.

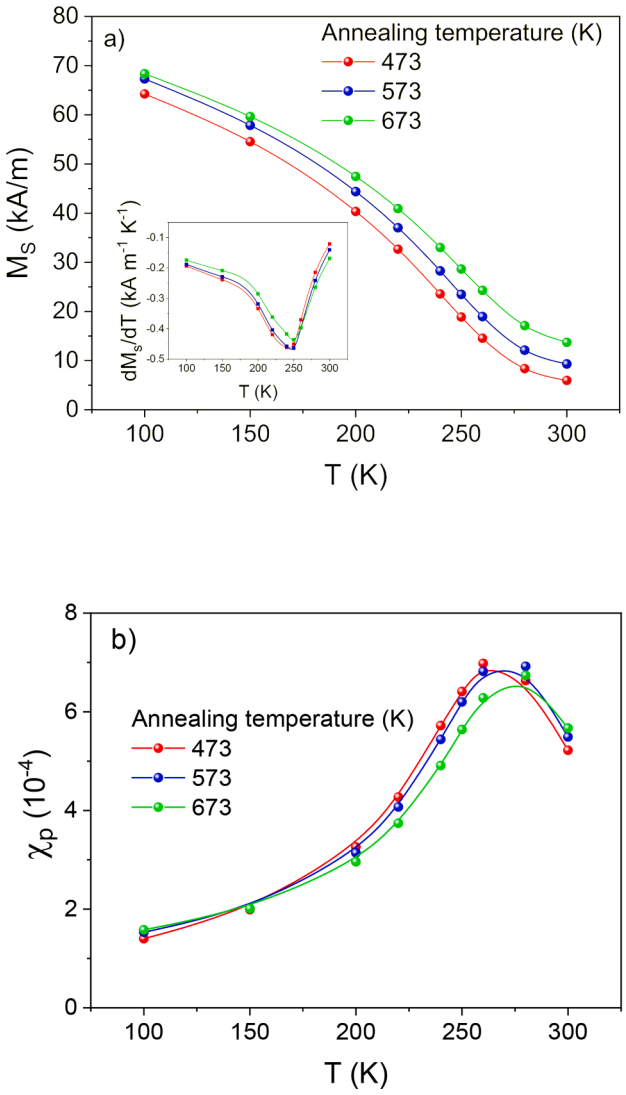

Fig. 6. Parameters obtained from the approach to saturation of the magnetization curves of Fig. 5 of the powders heated up until the indicated temperatures. a) Specific saturation magnetization and dM_S/dT curves (inset), where T_{inf} corresponds to the minimum. b) Paramagnetic susceptibility curves from the law of approach to saturation. Lines are guide for the eyes.

results. It has been shown that a significant change in the magnetization of as-milled powders occurs only when the powders are heated up above 800 K [7,30]. No more transitions have been observed in the range of temperature and magnetic fields applied to the powders. However, significant variations in the magnetization can be observed with the increase in the temperature of the thermal treatments. In this sense, magnetization does not fall to zero in none of the cases analyzed due to the existence of a certain α-Fe phase contribution, which has a much higher Curie temperature than those of the amorphous one (specific magnetization at 400 K increases from 4 to 13 kA/m as annealing temperature increases from 473 to 573 K in agreement with the increase observed in the ferromagnetic area from Mössbauer spectroscopy). As the annealing temperature increases, the drop of the magnetization at the Curie temperature decreases because of the growth of the α-Fe fraction, i.e. the difference between the magnetization before and after the Curie transition of the amorphous phase is reduced with the thermal treatment, in agreement with the evolution of the Mössbauer fits. Accordingly, the magnetization at low temperatures decreases due to the Fe depletion of the amorphous phase as the annealing temperature increases.

The applied field of 100 Oe (to measure the curves presented in Fig. 4a) is high enough to exceed the coercive field but low enough to allow the observation of a sufficiently pointed magnetic transition at the Curie temperature, T_C. This parameter has been estimated as the inflexion point of the magnetization as a function of temperature, (minimum in dM/dT curves, see b). Although the range of temperature at which dM/dT deflects from zero is considerable, typical for systems in which a Curie temperature distribution exists, a clear tendency can be observed: T_C increases with the increase of the annealing temperature. In fact, it is well known that T_C is strongly dependent on Fe content and the local atomic order in Fe-Zr amorphous compounds [31,32]. In this sense, it has been reported that in Fe-based amorphous alloys, with non-magnetic atom substitution, T_C increases as Fe content decreases in the alloy [30]. The increase of T_C, in this composition range, is due to a drop of the interatomic distances or to an increase of the Fe content. However, the thermal treatment of the sample involves an increase from 6 to 12% of α-Fe phase, as determined by Mössbauer spectroscopy (see Table 1). Therefore, the amorphous matrix of the annealed powders exhibits a slight impoverishment of the Fe content. It is verified by the enhancement of the magnetization remaining above the T_C of the

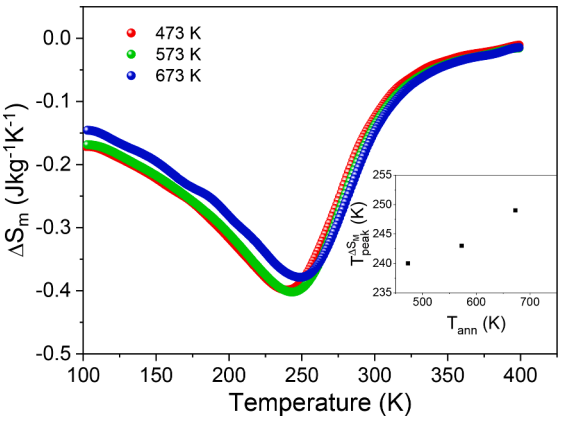

Fig. 7. Variation of ΔS_M with temperature (calculated for 1 T field change) for the studied amorphous alloys close to Curie temperature. Inset shows the evolution of maximum of ΔS_M with temperature.

amorphous structure (see Fig. 4a). Moreover, with the increase of the annealing temperature, the dM/dT curves become narrower. This fact could be ascribed to the release of the stresses accumulated in the amorphous powder during the milling process and the reduction of the impurities due to the nucleation of α-Fe crystallites.

Fig. 5 shows the hysteresis loops of the studied powders recorded at different temperatures from 100 to 300 K. As expected, all the samples exhibit a similar trend, characterized by a quick increase of the magnetization at low fields. This behavior of the hysteresis loops agrees with the expected soft-magnetic nature of the studied alloys.

The extracted values of saturation magnetization, $M_S(T)$, and the paramagnetic susceptibility, $\chi_p(T)$, of the hysteresis loops are displayed in Fig. 6. These parameters have been determined by fitting the experimental high-field magnetization curves ($\mu_0 H \geq 1$ T) to the linear version of law of approach to saturation [33]. $M_S(T)$ curves fall with the evolution of the temperature due to the ferro-paramagnetic transition of the amorphous phase. The growth of M_S as the annealing temperature increases is in agreement with the gradual rise of the α-Fe phase in the sample, with a higher magnetization than that of the amorphous structure. These results are in agreement with those obtained by Mössbauer spectroscopy. The inset of the Fig. 6a depicts the dM_S/dT curves, whose minimum, T_{inf}, is usually approximated to the Curie temperature. On the other hand, $\chi_p(T)$ curves exhibit a maximum, $T^{\chi_p}_{peak}$, that slightly shifts to higher temperatures with the increase of the annealing temperature. The divergence between T_{inf} and $T^{\chi_p}_{peak}$ found in our results indicates the presence of a distribution of transition temperatures [34]. Although a method to determine the parameters of this distribution was recently proposed using T_{inf} and $T^{\chi_p}_{peak}$ [34], both parameters need to better defined, avoiding a quantitative analysis of the distribution.

Fig. 7 presents the magnetic entropy change, ΔS_M, of the studied samples as a function of temperature for a maximum applied field change of 1 T. The $M(T,H)$ data were obtained on cooling cycles as a function of temperature at each magnetic field, being a temperature interval of 1 K and the ΔS_M was determined using a numerical approximation to the Maxwell relation. Demagnetizing field has not been taken into account and a negligible effect on $\Delta S_M(T)$ curves is assumed [22]. No significant differences can be observed between the different samples, reaching a maximum value of about 0.45 $Jkg^{-1}K^{-1}$ at 233 K for the sample as-milled. This maximum value slightly shifts to higher temperatures with the increase of the annealing temperature, in agreement with the results presented above. Although the obtained values of ΔS_M are similar to those found in the literature for samples with the same compositions obtained by mechanical milling, the observed values are modest when they are compared with amorphous ribbon samples of a similar composition produced by rapid quenching techniques (see table 2) [35,36]. It is also noted that the width of $\Delta S_M(T)$ curves decreases for rapidly quenched samples, suggesting a stronger inhomogeneity in the samples prepared by milling [37]. Recently, the C-doping of Fe-Zr amorphous alloys have been investigated in order to improve the magnetocaloric response of these materials through tuning the Curie temperature close to room temperature and achieving an enhancement of ΔS_M [38].

4. Conclusions

Relaxation of the amorphous structure of $Fe_{70}Zr_{30}$ amorphous alloy prepared by mechanical alloying has been investigated by means of annealing at temperatures below the devitrification temperature. The annealing treatments retain the amorphous structure of the alloy, detected by X-ray diffraction. However, they induce the initiation of nucleation of α-Fe crystallites, as estimated by Mössbauer spectra, which need one ferromagnetic and one paramagnetic contribution to be successfully fitted. Consequently, the amorphous alloy suffers a depletion in Fe content. This fact is verified by the augmentation of the magnetization persisting above the amorphous alloy's ferromagnetic-paramagnetic transition and the Curie temperature increase. Finally, the narrowing of the derivative curves of the magnetization with the annealing treatment suggests that, despite the partitioning of Fe to the nucleation of the α-Fe phase, the amorphous phase of the annealed samples is more chemically and structurally homogeneous than that of the original precursor.

CRediT authorship contribution statement

A.F. Manchón-Gordón: Conceptualization, Data curation, Investigation, Formal analysis, Resources, Writing – original draft. **J.S. Blázquez:** Conceptualization, Methodology, Supervision, Writing – review & editing, Resources. **M. Kowalczyk:** Data curation, Supervision,

Table 2
Experimental values of $|\Delta S_M|$ for FeZr based amorphous alloys prepared by different techniques.

Composition	Technique	T_{ann} (K)	T_C (K)	ΔH (T)	$\lvert\Delta S_M\rvert$ ($Jkg^{-1}K^{-1}$)	Reference
$Fe_{70}Zr_{30}$	Mechanical alloying	as-milled	235	1.0	0.45	[12]
		473	238	1.0	0.40	This work
		573	240	1.0	0.40	This work
		673	244	1.0	0.38	This work
$Fe_{70}Zr_{30}$	Mechanical alloying		244	1.5	~0.4	[23]
$Fe_{91}Zr_9$	Rapid quenching		233	1.5	1.22	[39]
$Fe_{90}Zr_{10}$	Rapid quenching		245	1	0.87	[33]
$Fe_{89}Zr_{11}$	Rapid quenching		263	1.8	1.3	[34]
$Fe_{93}Zr_7$	Sputtering		160	1.5	~0.7	[38]
$(Fe_{93}Zr_7)_{0.89}C_{0.11}$	Sputtering		311	1.5	~1	
$Fe_{88}Gd_2Zr_{10}$	Rapid quenching		285	1.5	1.4	[40]

Writing – review & editing. **J.J. Ipus:** Data curation, Supervision, Writing – review & editing. **T. Kulik:** Resources, Writing – review & editing. **C.F. Conde:** Resources, Methodology, Supervision, Writing – review & editing.

Declaration of Competing Interest

The authors declare that they have no known competing financial interests or personal relationships that could have appeared to influence the work reported in this paper.

Data availability

No data was used for the research described in the article.

Acknowledgements

This work was supported by the PAI of the Regional Government of Andalucía and by Junta de Andalucía-Consejería de Transformación Económica, Industria, Conocimiento y Universidades (proyect ProyExcel_00360). VI and VII-PPUS from University of Seville is also acknowledged.

References

[1] M.E. McHenry, M.A. Willard, D.E. Laughlin, Amorphous and nanocrystalline materials for applications as soft magnets, Prog. Mater Sci. 44 (4) (1999) 291–433.
[2] K. Hono, Nanoscale microstructural analysis of metallic materials by atom probe field ion microscopy, Prog. Mater Sci. 47 (6) (2002) 621–729.
[3] K. Balakrishnan, P.D. Babu, V. Ganesan, R. Srinivasan, S.N. Kaul, Magnetoelastic study of amorphous Fe90+xZr10−x alloys, J. Magn. Magn. Mater. 250 (2002) 110–122.
[4] I. Vincze, D. Kaptas, T. Kemény, L. Kiss, J. Balogh, Temperature and external magnetic field dependence of the spin freezing in amorphous Fe93Zr7, J. Magn. Magn. Mater. 140 (1995) 297–298.
[5] D. Mishra, A. Perumal, A. Srinivasan, Magnetic properties of mechanically alloyed Fe100− xZrx (20⩽ x⩽ 35) powder, J Phys D Appl Phys 41 (21) (2008), 215003.
[6] G. Concas, F. Congiu, G. Spano, M. Bionducci, Investigation of the ferromagnetic order in crystalline and amorphous Fe2Zr alloys, J. Magn. Magn. Mater. 279 (2–3) (2004) 421–428.
[7] A.F. Manchón-Gordón, J.J. Ipus, J.S. Blázquez, C.F. Conde, A. Conde, P. Svec, Study of the kinetics and products of the devitrification process of mechanically amorphized Fe70Zr30 alloy, J. Alloys Compd. 825 (2020), 154021.
[8] V. Franco, J.S. Blazquez, B. Ingale, A. Conde, The Magnetocaloric Effect and Magnetic Refrigeration Near Room Temperature: materials and Models, Annu. Rev. Mater. Res. (2012) 305–342.
[9] S.Y. Dan'kov, A.M. Tishin, V.K. Pecharsky, K.A. Gschneidner, Magnetic phase transitions and the magnetothermal properties of gadolinium, Phys. Rev. B 57 (6) (1998) 3478–3490.
[10] A. Planes, L. Manosa, X. Moya, T. Krenke, M. Acet, E.F. Wassermann, Magnetocaloric effect in Heusler shape-memory alloys, J. Magn. Magn. Mater. 310 (2) (2007) 2767–2769.
[11] I. Skorvanek, J. Kovac, Magnetocaloric behaviour in amorphous and nanocrystalline FeNbB soft magnetic alloys, Czech. J. Phys. 54 (2004) D189–D192.
[12] A.F. Manchón-Gordón, J.J. Ipus, L.M. Moreno-Ramírez, J.S. Blázquez, C.F. Conde, V. Franco, A. Conde, Correction of the shape effect on magnetic entropy change in ball milled Fe70Zr30 alloys, J. Alloys Compd. (2018).
[13] V. Franco, A. Conde, Scaling laws for the magnetocaloric effect in second order phase transitions: from physics to applications for the characterization of materials, International Journal of Refrigeration-Revue Internationale Du Froid 33 (3) (2010) 465–473.
[14] T. Malakhova, Z. Alekseyeva, The Zr-Fe phase diagram in the range 20–40 at.% Fe and the crystalline structure of the intermetallic compound Zr3Fe, Journal of the Less Common Metals 81 (2) (1981) 293–300.
[15] M. Granovsky, D. Arias, Intermetallic phases in the iron-rich region of the ZrFe phase diagram, J. Nucl. Mater. 229 (1996) 29–35.
[16] L. Schultz, Formation of amorphous metals by mechanical alloying, Mater. Sci. Eng. 97 (1988) 15–23.
[17] K. Unruh, C. Chien, Magnetic properties and hyperfine interactions in amorphous Fe-Zr alloys, Phys. Rev. B 30 (9) (1984) 4968.
[18] G. Herzer, Modern soft magnets: amorphous and nanocrystalline materials, Acta Mater. 61 (3) (2013) 718–734.
[19] R. Pizarro, J. Garitaonandia, F. Plazaola, J. Barandiaran, J. Greneche, Magnetic and Mössbauer study of multiphase Fe-Zr amorphous powders obtained by high energy ball milling, J. Phys. Condens. Matter 12 (13) (2000) 3101.
[20] A. Gupta, M. Gupta, S. Chakravarty, R. Rüffer, H.-.C. Wille, O. Leupold, Fe diffusion in amorphous and nanocrystalline alloys studied using nuclear resonance reflectivity, Phys. Rev. B 72 (1) (2005), 014207.
[21] M. Alouhmy, R. Moubah, G. Alouhmy, M. Abid, H. Lassri, Effects of hydrogen implantation on the magnetocaloric properties of amorphous FeZr films, Vacuum 186 (2021), 110063.
[22] A.F. Manchón-Gordón, J.J. Ipus, L.M. Moreno-Ramírez, J.S. Blázquez, C.F. Conde, V. Franco, A. Conde, Correction of the shape effect on magnetic entropy change in ball milled Fe70Zr30 alloys, J. Alloys Compd. 765 (2018) 437–443.
[23] J.S. Blazquez, V. Franco, A. Conde, Enhancement of the magnetic refrigerant capacity in partially amorphous Fe70Zr30 powders obtained by mechanical alloying, Intermetallics 26 (2012) 52–56.
[24] J. Blázquez, J. Ipus, C. Conde, A. Conde, Comparison of equivalent ball milling processes on Fe70Zr30 and Fe70Nb30, J. Alloys Compd. 536 (2012) S9–S12.
[25] A.F. Manchón-Gordón, J.J. Ipus, J.S. Blázquez, C.F. Conde, A. Conde, Evolution of Fe environments and phase composition during mechanical amorphization of Fe70Zr30 and Fe70Nb30 alloys, J. Non Cryst. Solids 494 (2018) 78–85.
[26] J.S. Blázquez, A.F. Manchón-Gordón, J.J. Ipus, C.F. Conde, A. Conde, On the use of JMAK theory to describe mechanical amorphization: a comparison between experiments, Num. Sol. Simulations, Metals (2018).
[27] A.F. Manchón-Gordón, J.J. Ipus, J.S. Blázquez, C.F. Conde, A. Conde, Influence of milling time on the homogeneity and magnetism of a Fe70Zr30 partially amorphous alloy: distribution of curie temperatures, Materials (Basel) 13 (2) (2020) 490.
[28] R.A. Brand, J. Lauer, D.M. Herlach, The evaluation of hyperfine field distributions in overlapping and asymmetric mossbauer-spectra: a study of the amorphous alloy PD77.5-XCU6SI16.5FEX, J. Phys. F-Metal Phys. 13 (3) (1983) 675–683.
[29] J.S. Blazquez, J.J. Ipus, V. Franco, C.F. Conde, A. Conde, Extracting the composition of nanocrystals of mechanically alloyed systems using Mossbauer spectroscopy, J. Alloys Compd. 610 (2014) 92–99.
[30] A.F. Manchón-Gordón, R. López-Martín, A. Vidal-Crespo, I.J. J, J.S. Blázquez, C. F. Conde, A. Conde, Distribution of transition temperatures in magnetic transformations sources effects procedures to extract information from experimental, Data, Metals (2020).
[31] R. Pizarro, J.S. Garitaonandia, F. Plazaola, J.M. Barandiaran, J.M. Greneche, Magnetic and Mossbauer study of multiphase Fe-Zr amorphous powders obtained by high energy ball milling, J. Phys.: Condens. Matter 12 (13) (2000) 3101–3112.
[32] R. Moubah, A. Zamani, A. Olsson, S. Shi, A. Hallén, S. Carlson, D. Arvanitis, P. Nordblad, B. Hjörvarsson, P. Jönsson, Soft room-temperature ferromagnetism of carbon-implanted amorphous Fe93Zr7 films, Appl. Phys. Express 6 (5) (2013), 053001.
[33] J.M. Coey, Magnetism and Magnetic Materials, Cambridge university press, 2010.
[34] A.F. Manchón-Gordón, L.M. Moreno-Ramírez, J.J. Ipus, J.S. Blázquez, C.F. Conde, V. Franco, A. Conde, A procedure to obtain the parameters of Curie temperature distribution from thermomagnetic and magnetocaloric data, J. Non Cryst. Solids 520 (2019), 119460.
[35] T. Dang Thanh, Y. Yu, P. Thanh, N. Yen, N. Dan, T.-.L. Phan, A. Grishin, S. Yu, Magnetic properties and magnetocaloric effect in Fe90− x Ni x Zr10 alloy ribbons, J. Appl. Phys. 113 (21) (2013), 213908.
[36] D. Mishra, M. Gurram, A. Reddy, A. Perumal, P. Saravanan, A. Srinivasan, Enhanced soft magnetic properties and magnetocaloric effect in B substituted amorphous Fe–Zr alloy ribbons, Mater. Sci. Eng. 175 (3) (2010) 253–260.
[37] L.M. Moreno-Ramirez, J.J. Ipus, V. Franco, J.S. Blazquez, A. Conde, Analysis of magnetocaloric effect of ball milled amorphous alloys: demagnetizing factor and Curie temperature distribution, J. Alloys Compd. 622 (2015) 606–609.
[38] A. Charkaoui, R. Moubah, M. Bouhbou, H. Lassri, A. Elouafi, P.E. Jönsson, Critical behavior and magnetocaloric effect in C-implanted Fe93Zr7 amorphous films, Solid State Commun. 316-317 (2020), 113962.
[39] K.S. Kim, Y.S. Kim, J. Zidanic, S.G. Min, S.C. Yu, Magnetocaloric effect in as-quenched and annealed Fe91-xYxZr9 (x=0.5, 10) alloys, Physica Status Solidi a-Appl. Mater. Sci. 204 (12) (2007) 4096–4099.
[40] T.D. Thanh, N.H. Yen, N.H. Duc, T.L. Phan, N.H. Dan, S.C. Yu, Large magnetocaloric effect around room temperature in amorphous Fe-Gd-Zr alloy ribbon with short-range interactions, J. Electron. Mater. 45 (5) (2016) 2608–2614.